Complicated magnetic structure and its strong correlation with the anomalous Hall effect in Mn_{3}Sn

Yuzhu Song, Yiqing Hao, Shaobo Wang, Ji Zhang, Qingzhen Huang, Xianran Xing, and Jun Chen

Phys. Rev. B **101**, 144422 — Published 16 April 2020

DOI: 10.1103/PhysRevB.101.144422

Complicated magnetic structure and its strong correlation with the anomalous Hall effect in Mn_3Sn

Yuzhu Song,[1] Yiqing Hao,[2] Shaobo Wang,[3] Ji Zhang,[4] Qingzhen Huang,[5] Xianran Xing[6] and Jun Chen*,[1]

[1]Beijing Advanced Innovation Center for Materials Genome Engineering, and School of Mathematics and Physics, University of Science and Technology Beijing, Beijing 100083, China

[2]State Key Laboratory of Surface Physics and Department of Physics, Fudan University, Shanghai 200433, China

[3]Institute of Microstructure and Property of Advanced Materials, Beijing University of Technology, Beijing 100124, China

[4]School of Materials Science and Engineering, Nanjing University of Science and Technology, Nanjing 210094, China

[5]NIST Center for Neutron Research, National Institute of Standards and Technology, Gaithersburg MD, 20899-6102, USA

[6]Beijing Advanced Innovation Center for Materials Genome Engineering, and Institute of Solid State Chemistry, University of Science and Technology Beijing, Beijing 100083, China

* Corresponding author: junchen@ustb.edu.cn

Abstract:

The large anomalous Hall effect (AHE) has recently been found in noncollinear antiferromagnet Mn_3Sn. However, the complex magnetic structure and its correlation with the AHE remain unclear. Here, we investigate the magnetic structure of Mn_3Sn completely by means of both the temperature and magnetic field dependence of neutron power diffraction. This study establishes the possible incommensurate magnetic structure models, and extracts the temperature evolution of the magnetic moment of the Mn atom over the whole temperature range for Mn_3Sn. The large AHE of polycrystalline bulk Mn_3Sn is measured in detail. By comparing the temperature dependence of the spontaneous component of the AHE and the magnetic moment, direct experimental evidence reveals that the triangular antiferromagnetic ordered moment of the Mn atom controls the change in the AHE of Mn_3Sn. This study provides the possibility to control the AHE of functional materials via changing the magnetic structure.

I. INTRODUCTION

Due to its remarkable magnetic, structural, and electrotransport properties, the noncollinear chiral antiferromagnet Mn_3Sn has attracted extensive attention. In the past few years, scientists have observed the excellent performance and interesting phenomena of Mn_3Sn, such as a large anomalous Hall effect (AHE) at room temperature,[1] large anomalous Nernst effect at room temperature,[2] large

magneto-optical Kerr effect,[3] magnetic and magnetic inverse spin Hall effects,[4] and magnetic Weyl fermions.[5] In particular, the large AHE in Mn_3Sn has reaffirmed the current understanding of the Hall effect. It is well known that the AHE of a ferromagnet conductor is proportional to its magnetization. For an antiferromagnet, no AHE should be observed in the zero field because of the lack of net magnetization. However, a large anomalous Hall conductivity has been found in antiferromagnet Mn_3Sn, even at the same order of magnitude as for ferromagnetic conductors.[1] The AHE had not been observed in antiferromagnets until the discovery of Mn_3Sn. The rich physical properties of compound may be inseparable from its special structure.

The magnetic structure of Mn_3Sn is complicated and sensitive to its composition and synthesis conditions (the annealing temperature).[6] H. Ohmori etc. found a triangular screw spin structure below 250 K, and the modulated phase disappeared when the sample was quenched from 900 °C.[7] J.W. Cable etc. found two coexistent modulated phases in an inhomogeneous Mn_3Sn alloy.[8] According to the previous study, the variable magnetic structure of Mn_3Sn closely controls its AHE property. For example, due to the absence of an incommensurate magnetic structure, a large anomalous Hall conductivity appears in Mn_3Sn over a wide temperature range.[1] When the commensurate state becomes an incommensurate magnetic structure below T = 275 K, the large AHE vanishes suddenly.[9] Therefore, to better control the Hall effect, it is necessary to determine the detailed magnetic structure of Mn_3Sn and establish a relation to the AHE over the whole temperature range.

In this study, we completely determined the complicated magnetic structure of

Mn_3Sn by means of neutron powder diffraction (NPD) as a function of the temperature and magnetic field. The possible incommensurate magnetic structure models are established in this study. The stability of incommensurate and commensurate magnetic structures under an external magnetic field is studied by the variable magnetic field NPD at different temperatures. By studying the temperature evolution magnetic moment of the Mn atom and the anomalous Hall effect, direct experimental evidence reveals a strong connection between the anomalous Hall effect and the magnetic structure of Mn_3Sn over the whole temperature range.

II. EXPERIMENTAL SECTION

The polycrystalline sample of Mn_3Sn was prepared using arc-melting methods.[10] Variable temperature neutron diffraction patterns with a wave length 2.41 Å were collected using the high-intensity Wombat diffractometer of the Australian Nuclear Science and Technology Organisation (ANSTO). The variable magnetic field NPD patterns at different temperatures were measured in the BT-1 neutron powder diffractometer at the NIST Center for Neutron Research. The wavelength of the neutron beam was 1.5397 Å. During the applied-field neutron experiment, the powder samples are pressed into pellets and fixed in the sample can, so the grain re-orientation can be avoided. The magnetic properties were measured in a Quantum Design Magnetic Property Measurement System (MPMS). Both Hall and longitudinal resistivity were measured by a standard four-probe method using a commercial Quantum Design Physical Property Measurement System (PPMS). The magnetic

structure refinements for all NPD data were analyzed by FULLPROF software.[11] SARAH[12] and BASIREPS in FULLPROF were utilized for the magnetic representational analysis.

III. RESULTS AND DISCUSSION

The polycrystalline ingots of Mn_3Sn were prepared by arc melting. The crystal structure was identified by variable temperature NPD, namely, a single phase with a hexagonal Ni_3Sn-type structure (space group: $P6_3/mmc$) over the whole temperature range. Mn and Sn atoms occupy Wyckoff sites 6h (x, $2x$, 1/4) and 2c (1/3, 2/3, 1/4), respectively. To study the macroscopic magnetic behavior of Mn_3Sn, the temperature dependence of the magnetization (field-cooling modes, FC) was measured under different external magnetic fields (Fig. 1(a)). One can see that the system has two obvious magnetic transitions at T_S = 190 K and above 400 K, which is similar to the previous report.[7] A previous study revealed the existence of an inverse triangular antiferromagnetic (AFM) structure below T_N = 420 K, and the triangular state transforms into an incommensurate magnetic spin at T_S.[13] Below T_g = 50 K, there is an upturn in magnetization curves with decreasing temperature. As previously reported, this phenomenon is caused by glassy ferromagnetism,[14] but the detailed magnetic structure is still unknown. Furthermore, the tendencies of the FC curves and the magnetic transition temperature are hardly changed by the different magnetic fields. Only a small amount of magnetization can be enhanced by increasing the filed, which verifies the stability of these magnetic states.

The isothermal magnetization (M-H) of Mn_3Sn was measured at selected temperatures that cover the temperature range of different magnetic states (Fig. 1(b)). As can be seen, no M-H curves can saturate under a high magnetic field, and the ferromagnetic hysteresis phenomenon appears in the M-H curves at high temperature, which means that weak ferromagnetism (WF) exists in the inverse triangular antiferromagnetic state of Mn_3Sn. Previous first-principles calculations proved that the WF component is formed by the noncollinearity of the atomic spin and orbital moments of Mn atoms.[15] The hysteresis disappears with the transformation of the triangular state into an incommensurate magnetic spin below 190 K. The study of macroscopic magnetism on Mn_3Sn gives us a general understanding of its magnetic structure.

Most studies note the macroscopic transition from the inverse triangular state to the modulated phase in Mn_3Sn, but the detailed magnetic structure has not been established over the whole temperature range. Neutron diffraction is the best approach to analyze incommensurate magnetic structures. Therefore, the temperature dependence of high-intensity NPD data was measured at 10-500 K to study the microscopic magnetic structure of Mn_3Sn. Contour plots of the (101) and $(101)_{\pm}$ NPD profile intensities as a function of temperature for Mn_3Sn are depicted in Fig. 2(a). Clearly, there are two satellite reflections on each side of (101) appearing at temperatures below 250 K, which can be signed to $(101)_{\pm}$. The satellite reflections were also found in the previous NPD study on Mn_3Sn, but the detailed magnetic structure model and the change in moments were not determined.[7,8] To better

observe the change in magnetic peaks, we calculated the temperature dependence of the integrated intensity of the satellite and the fundamental peaks (Fig. 2(b)). Above T_N = 430 K, Mn_3Sn is a disordered paramagnetic state; thus, the fundamental peak (101) maintains a nearly constant nuclear intensity. Below T_N, the inverse triangular AFM order appears, and the intensity of (101) increases to a maximum at 250 K. With decreasing temperature, the commensurate magnetic structure transforms into the modulated phase. The intensity of (101) begins to decrease, and then retains an almost similar intensity to that of nuclear peaks below 190 K. Meanwhile, the satellite reflections appear at 250 K. Since the magnetic phase completely becomes an incommensurate magnetic spin, the satellite reflections remain nearly constant below 190 K. Therefore, the magnetic phase diagram of Mn_3Sn can be divided into four regions in this study, i.e., (1) 10 < T < 190 K, (2) 190 < T < 250 K, (3) 250 < T < 430 K, and (4) T > 430 K. Note that different magnetic transition temperatures could have occurred in the previous studies, due to the difference in alloy composition, synthesis conditions, and form of samples.[1,9,16]

According to the change in magnetic Bragg reflections, the magnetic structure of Mn_3Sn can be established by magnetic representational analysis. First, at 250 < T < 430 K, the inverse triangular AFM structure has been reported by many studies, which is similar to that of Mn_3Ge.[17] As depicted in the inset of Fig. 3(d), all the Mn moments are along the [110] direction at the *a*-*b* plane, and the spins rotate by 120° with an opposite vector chirality. This triangular magnetic order is very special and can break the in-plane hexagonal symmetry of the lattice; thus, anomalous physical

properties may occur in Mn_3Sn.

Second, at 10 < T < 190 K, the intensity of (101) remains almost similar to that of the nuclear peak; thus, the commensurate spin disappeared completely in this temperature region. Based on the positions of the satellite reflections, the propagation vector of the incommensurate spin can be determined to be approximately (0, 0, 0.08). The magnetic representational analysis of the space group $P\,6_3/mmc$ was carried out using SARAH and BASIREPS with this propagation vector. According to the agreement that computed results have with the experimental data, the best irreducible representations of magnetic vectors can be established. Eventually, two magnetic components can consist of this incommensurate state. One is the triangular in-plane component, which is similar to the AFM structure at high temperature, and the other is up-down-0 in the *c*-direction (Fig. 3(a) and 3(b)). It should be noted that both components can be combined with either cosine or cycloidal magnetic structures. The right side of 1×1×3 supercell is the periodicity beyond three unit cells along the c axis, in which only the site of Mn atom is shown. The Mn spin rotates along the *c* axis, with a cosine and cycloidal arrangement. Therefore, the periodicity is similar to that of a typical helical magnetic structure with a period of approximately 12c along the *c* axis, which is nearly 5.5 nm. Due to the contribution to the magnetic Bragg reflections being the same, neither the cosine nor cycloidal structure model can be distinguished by the NPD measurement. To simplify things, we chose only the cosine structure to address all the data in the present study. The NPD data at all temperatures can be fitted well by the above-proposed magnetic structure (Fig. 3(c) and 3(d)). The

proposed incommensurate magnetic structure of Mn_3Sn in this study is different from the previous report, in which two coexistent modulated phases were found due to the inhomogeneous distribution. That modulated phase was believed to be a severely distorted helix with multilayer blocks of moments tending toward alignment along the easy six-fold axes in the basal plane.[8]

The above macroscopic magnetism shows that there is a spin-glass state below T_g = 50 K. However, the NPD patterns show nothing unusual below 50 K, and the satellite reflections remain nearly constant to 10 K. Thus, there is the coexistence of the glassy component and the long-range helical magnetic structure below 50 K. The spin-glass state has no periodicity, in which magnetic signals cannot be detected by NPD, but can be detected by a macroscopic magnetic measurement. It was reported that because of spin canting towards the *c* axis the spin-glass state appears with a *c*-axis ferromagnetic component[18, 19] According to our magnetic structure analysis, the *c*-axis ferromagnetic component of the glass phase may have some connection with the *c*-direction magnetic components of the incommensurate spin. The appearance of the glassy state needs further study.

The NPD patterns of different magnetic structures are simulated in Fig. 4(a). The magnetic contribution to the NPD patterns of different magnetic states can be observed clearly when compared with the nuclear peaks. The most obvious difference between the triangular and cosine magnetic structures is the magnetic contribution to the (101) reflections. The cosine magnetic state does not contribute to the (101) reflections, while the triangular state does. The temperature dependence of the

magnetic moments is extracted from the variable temperature NPD patterns (Fig. 4(b)). The cosine magnetic state has two components along the *a* and *c* axes, respectively. The magnetic moments of Mn along the *a* (M_a) and *c* (M_c) axes are different in not only magnitude but also decreasing temperature. Both remain constant at low temperature and sharply decrease around T_S. The change in the triangular AFM magnetic moment (M_{Tri}) seems opposite that of the cosine state. Below T_N, the M_{Tri} increases with decreasing temperature up to 250 K, and then decreases to zero at 190 K. The tendency of the magnetic moments is similar to that of the magnetic Bragg reflections, which further verifies the reasonableness of the proposed magnetic structure. The propagation vectors of the cosine state are independent of temperature, always being near (0, 0, 0.08) (Fig. 4(c)). As shown in Fig. 4(d), the temperature dependence of the lattice parameters increases with heating and has two inflections around the magnetic transition temperatures. The anomalous thermal expansion in Mn_3Sn originates from the magnetovolume effect.[10]

To study how the magnetic structure of Mn_3Sn is affected by external fields, the variable magnetic field NPD was measured at 190 K and 270 K, which correspond to the incommensurate and triangular magnetic structure regions, respectively (Fig. 2(c) and 2(d)). Obviously, with increasing magnetic field from 0 T to 7 T, all the NPD patterns have almost no change in either peak intensity or position. The result of the variable magnetic field NPD is in good accordance with the magnetization curves. Both indicate that the long-range magnetic structure of Mn_3Sn is very stable under a magnetic field.

As an antiferromagnet, it is unusual to find a large AHE in Mn_3Sn.[1] The large AHE of Mn_3Sn could have a close relationship with its complicated magnetic structure. To study the relation between the magnetic structure and anomalous Hall effect, the field dependence of the Hall resistivity ρ_H is measured at 5-400 K (selected temperatures are shown in Fig. 5(a)). The ρ_H exhibits a clear hysteresis loop, with the largest change $\Delta\rho_H \approx 5$ μΩcm at T = 235 K, which is comparable to those of the single-crystal Mn_3Sn and Mn_3Ge.[1,20] Below 190 K, ρ_H is nearly zero and linearly increases with B. The Hall resistivity usually consists of the normal and anomalous Hall effects, i.e., $\rho_H = R_0B + R_s\mu_0M$, where R_0 and R_s are the normal and anomalous Hall coefficients.[21] However, the conventional description of Hall resistivity cannot characterize that in the triangular antiferromagnet Mn_3Sn. According to the previous study, it is necessary to add another dominant contribution to the AHE, which can be labeled as ρ_{HAF}. Then the Hall resistivity of Mn_3Sn can written as $\rho_H = R_0B + R_s\mu_0M + \rho_{HAF}$. For the noncollinear AFM structure of a single-crystal, ρ_{HAF} appears only in *ab* components, and is absent when the field is parallel to the *c* axis. Therefore, it is easy to calculate each part of ρ_H for a single-crystal sample by measuring the Hall resistivity along different crystal axes. Since the Hall resistivity of this study is measured from a polycrystalline ingot sample, it is difficult to extract each component of the AHE. Therefore, the anomalous Hall resistivity of Mn_3Sn in the following discussion is the sum of $R_s\mu_0M$ and ρ_{HAF}.

To reveal the temperature dependence of the spontaneous component of the AHE, the Hall resistivity at zero field ($B = 0$) is extracted from the field dependence of the

ρ_H curves (Fig. 5(b)). Clearly, the ρ_H remains nearly zero up to 190 K, increases to a maximum at approximately 250 K, and then decreases with increasing temperature. The change in Hall resistivity seems similar to that of the magnetic structure. The zero-field Hall conductivity is calculated by σ_H (B = 0) = -ρ_H(B = 0) / ρ_{xx}^2(B = 0), where ρ_{xx} is the longitudinal resistivity. To obtain the Hall conductivity, the temperature evolution of ρ_{xx} is measured at B = 0 and B = 1T, respectively (Fig. 5(c)). The metallic behavior of Mn_3Sn is exhibited by the ρ_{xx}-T curves, and the magnetoresistance (MR) at 1T is very small (approximately -2.3%). Due to the low electron–phonon scattering in Mn_3Sn,[22] the longitudinal resistivity almost remains constant at T > 300 K, which is the near-zero temperature coefficient of resistivity (NZ-TCR).

The reason for the large AHE in a noncollinear AFM is still unclear. The theoretical predictions from Li et al. suggest that the nonvanishing Berry curvature arising from the noncollinear AFM is responsible for the observed large AHE.[13] In particular, the temperature evolution of the relationship between the magnetic structure and anomalous Hall effect remains ambiguous. To reveal the relationship between the magnetic structure and the anomalous Hall effect, the temperature evolution of the zero-field Hall conductivity and that of the triangular antiferromagnetic moment of Mn (M_{Tri}) are compared in Fig. 5(d). Obviously, there is a strong correlation between both M_{Tri} and σ_H (B = 0). At low temperature (below 190 K), it is a completely incommensurate state, and the triangular AFM moment is zero; thus, the AHE is absent. In comparison to previous studies, the large AHE can exist at

50 K due to the AFM phase stable above 50 K.[1] With increasing temperature from 190 K, the modulated phase gradually transforms into the commensurate state. The Hall conductivity increases synchronously with the formation of triangular AFM moments. The maximum zero-field Hall conductivity is 60 $\Omega^{-1}cm^{-1}$, which is reported in half of the previous studies on single-crystal Mn_3Sn.[1] Due to the thermal disturbance, the AFM spins gradually depart from the ordered distribution; thus, the average AFM moment decreases upon heating. Similarly, the zero-field Hall conductivity decreases, and eventually reduces to zero at the Néel temperature (T = 430 K). Therefore, the AHE of Mn_3Sn is controlled by the ordered moments of the Mn atoms, which is not related to the incommensurate state and the net magnetization of weak ferromagnetism. In comparison, the relation between AHE and magnetism is very similar to the correlation between negative thermal expansion and the magnetic moment.[23,24] Based on this relationship, the AHE of Mn_3Sn can be tuned by changing its magnetic structure.

IV. CONCLUSIONS

In summary, the complex magnetic structure of Mn_3Sn is determined by NPD over the whole temperature range. The visual incommensurate magnetic structure is built, i.e., the cosine and cycloidal models, and the temperature evolution of the magnetic moment of the Mn atom is extracted from NPD. By comparing the change in the magnetic moment of the Mn atom and the zero-field Hall conductivity as a function of temperature, direct experimental evidence reveals that the large AHE is controlled by

the ordered moment of the Mn atom. A comprehensive study of the complex magnetic structure is meaningful to better understand the remarkable magnetic, structural, and electrotransport properties of Mn_3Sn. This study on the relation between the magnetic structure and anomalous Hall effect is helpful for the design of other AHE functional materials.

ACKNOWLEDGMENTS

This work was supported by the National Natural Science Foundation of China (grant nos. 21825102, 21731001 and 21590793), and the Fundamental Research Funds for the Central Universities, China (FRF-TP-18-001C2). This research used resources of the Advanced Photon Source, a U.S. Department of Energy (DOE) Office of Science User Facility operated for the DOE Office of Science by Argonne National Laboratory under Contract No. DE-AC02-06CH11357. We thank Dr. Chinwei Wang to collect neutron powder diffraction data at the high-intensity diffractometer Wombat of the Australian Nuclear Science and Technology Organisation (ANSTO).

REFERENCES

[1] S. Nakatsuji, N. Kiyohara, and T. Higo, Nature **527**, 212 (2015).

[2] M. Ikhlas, T. Tomita, T. Koretsune, M. T. Suzuki, D. Nishio-Hamane, R. Arita, and S. Nakatsuji, Nat. Phys. **13**, 1085 (2017).

[3] T. Higo, H. Man, D. B. Gopman, L. Wu, T. Koretsune, O. M. van't Erve, and S. Patankar, Nat. photon. **12**, 73(2018)..

[4] M. Kimata, H. Chen, K. Kondou, S. Sugimoto, P. K. Muduli, M. Ikhlas, and Y. Otani, Nature **565**, 627 (2019).

[5] K. Kuroda, T. Tomita, M. T. Suzuki, C. Bareille, A. A. Nugroho, P. Goswami, and

R. Noguchi, Nat. Mater. **16**, 1090 (2017).

[6] E. Krén, J. Paitz, G. Zimmer, and É. Zsoldos, Phys. B+ C, **80**, 226-230 (1975).

[7] H. Ohmori, S. Tomiyoshi, H. Yamauchi, and H. Yamamoto, J. Magn. Magn. Mater. **70**, 249-251 (1987).

[8] J. W. Cable, N. Wakabayashi, and P. Radhakrishna, Solid State Commun. **88**, 161-166 (1993).

[9] N. H. Sung, F. Ronning, J. D. Thompson, and E. D. Bauer, Appl. Phys. Lett. **112**, 132406 (2018).

[10] Y. Song, Y. Qiao, Q. Huang, C. Wang, X. Liu, Q. Li, and X. Xing, Chem. Mater. **30**, 6236-6241 (2018).

[11] J. Rodríguez-Carvajal, Tutorial on magnetic structure determination and refinement using neutron powder diffraction and fullprof, (2014).

[12] A. S. Wills, Phys. B: Condens. Matter **276**, 680-681(2000).

[13] X. Li, L. Xu, L. Ding, J. Wang, M. Shen, X. Lu, and K. Behnia, Phys. Rev. Lett. **119**, 056601(2017).

[14] W. J. Feng, D. Li, W. J. Ren, Y. B. Li, W. F. Li, J. Li, and Z. D. Zhang, Phys. Rev. B **73**, 205105 (2006).

[15] L. M. Sandratskii, and J. Kübler, Phys. Rev. Lett. **76**, 4963 (1996).

[16] A. Markou, J. M. Taylor, A. Kalache, P. Werner, S. S. P. Parkin, and C. Felser, Phys. Rev. Mater. **2**, 051001 (2018).

[17] J. W. Cable, N. Wakabayashi, and P. Radhakrishna, Phys. Rev. B **48**, 6159 (1993).

[18] P. J. Brown, V. Nunez, F. Tasset, J. B. Forsyth, and P. Radhakrishna, J. Phys. Condens. Matter **2**, 9409 (1990).

[19] S. Tomiyoshi, S. Abe, Y. Yamaguchi, H. Yamauchi, and H. Yamamoto, J. Magn.

Magn. Mater. **54**, 1001-1002 (1986).

[20] A. K. Nayak, J. E. Fischer, Y. Sun, B. Yan, J. Karel, A. C. Komarek, and C. Felser, Sci. Adv. **2**, 1501870 (2016).

[21] N. Nagaosa, J. Sinova, S. Onoda, A. H. MacDonald, and N. P. Ong, Rev. Mod. Phys. **82**, 1539 (2010).

[22] S. Shafeie, S. Guo, P. Erhart, Q. Hu, and A. Palmqvist, Adv. Mater. **31**, 1805392 (2019).

[23] C. Wang, L. Chu, Q. Yao, Y. Sun, M. Wu, L. Ding, and Q. Huang, Phys. Rev. B **85**, 220103 (2012).

[24] S. Iikubo, K. Kodama, K. Takenaka, H. Takagi, and S. Shamoto, Phys. Rev. B **77**, 020409 (2008).

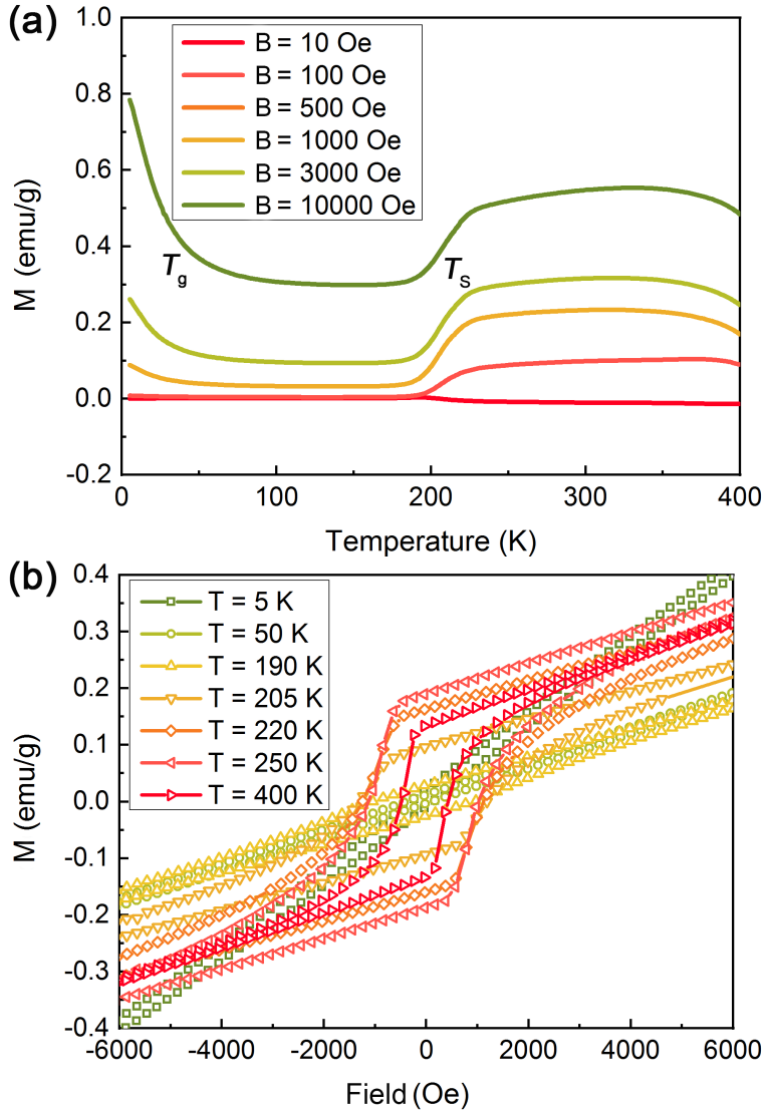

FIG. 1. (a) Magnetization as a function of the external magnetic field and temperature (field-cooling modes, FC), and (b) isothermal magnetization (M-H) at selected temperatures for Mn_3Sn.

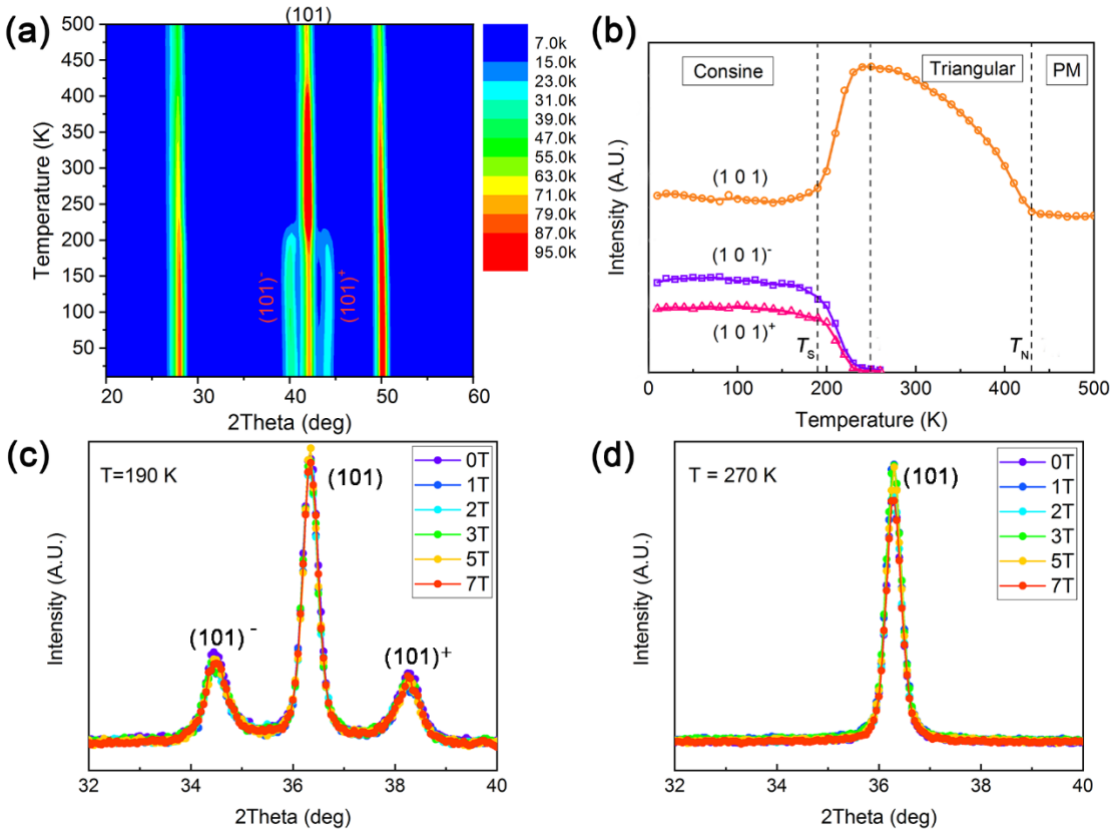

FIG. 2. (a) Contour plots of the (101) and $(101)_{\pm}$ NPD profile intensity as a function of temperature. (b) Temperature dependence of the integrated intensity of the satellite $(101)_{\pm}$ and the fundamental peaks (101). The NPD patterns for Mn_3Sn at (c) 190 K and (d) 270 K as a function of the magnetic field (H = 0 T, 1 T, 2 T, 3 T, 5 T, and 7 T).

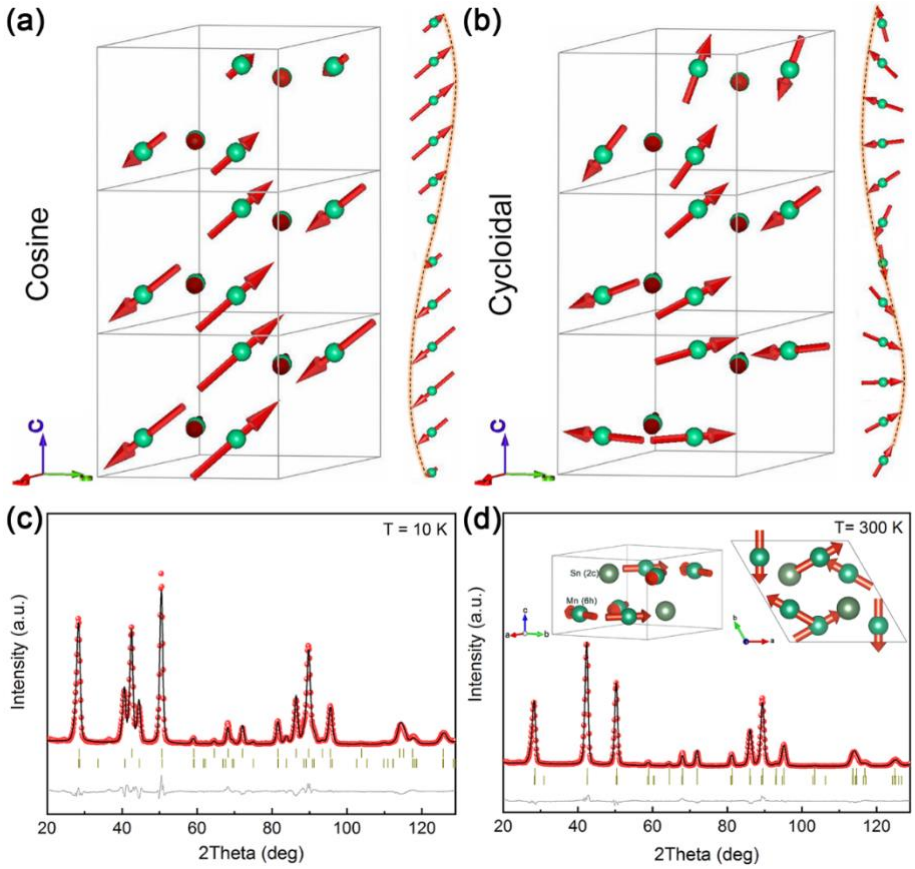

FIG. 3. The incommensurate magnetic structure of Mn_3Sn: (a) cosine and (b) cycloidal models. The right side of 1×1×3 supercell is the periodicity beyond three unit cells along the c axis, in which only the site of Mn atom is shown. Magnetic structure refinements of NPD patterns of Mn_3Sn using (c) the cosine model at T = 10 K and (d) the inverse triangular AFM model at T = 300 K. The inset of (d) is the inverse triangular AFM structure model.

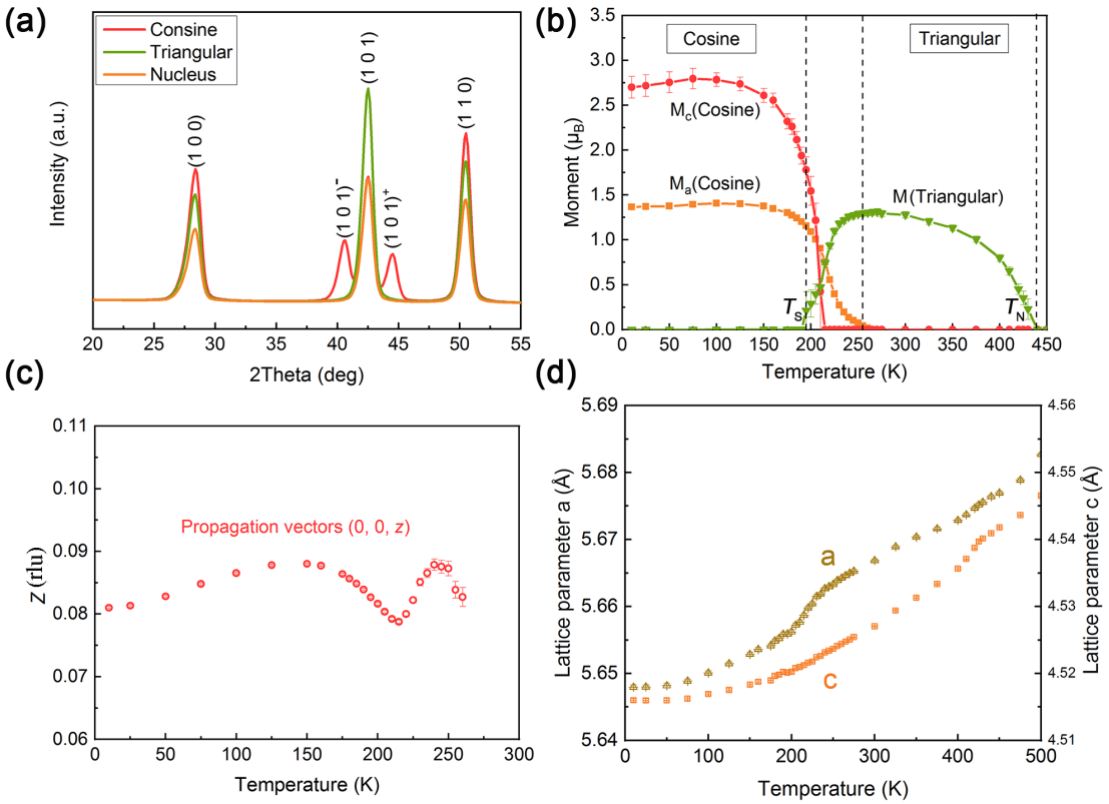

FIG. 4. (a) The simulated magnetic contribution to the NPD patterns from the cosine, triangular, and nucleus structures, respectively. (b) The component of the magnetic moment on different crystal axes, (c) propagation vectors of the modulated phase, and (d) lattice parameters as a function of temperature.

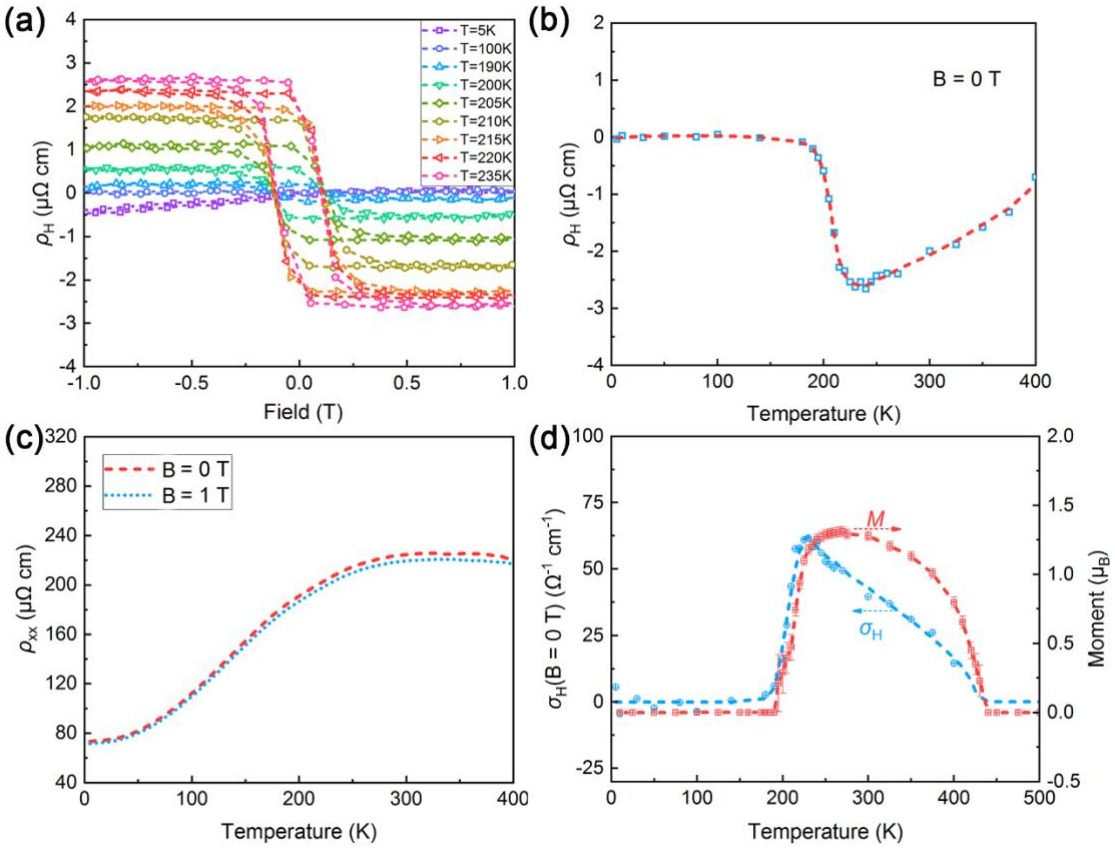

FIG. 5. (a) Field dependence of Hall resistivity ρ_H at selected temperatures, (b) temperature dependence of Hall resistivity at zero-field (B = 0), (c) temperature evolution of longitudinal resistivity (ρ_{xx}) measured at B = 0 and B = 1 T, and (d) the comparison between the zero-field Hall conductivity and triangular antiferromagnetic moment of Mn (M) as a function of temperature for Mn_3Sn.